KNOWLEDGE-BASED SOLUTIONS AS THEY APPLY TO THE GENERAL RADAR PROBLEM

H.D. Griffiths
Head, Department of Electronic and Electrical Engineering
University College London
Torrington Place, London WC1E 7JE, UK
Tel: +44 20 7679 7310; fax: +44 20 7388 9325; email: h.griffiths@ee.ucl.ac.uk

Keywords: radar, signal processing, adaptive processing, adaptive arrays, clutter, space-time adaptive processing, knowledge-based systems.

SUMMARY

This tutorial provides an introduction to the application of knowledge-based processing to the general radar problem. We interpret knowledge-based processing as the use of adaptivity and the exploitation of prior knowledge in such a way as to choose the optimum processing method in each case, and we interpret the general radar problem as the detection, classification and tracking of targets against a background of clutter and interference. As such the tutorial attempts to describe the nature of the general radar problem and the basic processing techniques that are used, and to show why knowledge-based signal processing may be advantageous, setting the scene for the subsequent tutorials covering CFAR detection, space-time adaptive processing, tracking, and emerging technologies. The fundamental concepts of matched filtering, superresolution and adaptive filtering are described, emphasizing the equivalence of time/frequency and aperture/angular domains, and introducing the concept of Space-Time Adaptive Processing. A description is given of some of the statistical clutter models in common use (Rayleigh, Ricean, Lognormal, Weibull and Compound-K), with practical examples of sea clutter and of land clutter which demonstrate that clutter is in general non-Gaussian and non-stationary, both in time and space. Two examples are given of the application of adaptive techniques to the suppression on nonhomogeneous clutter, showing that the performance of the adaptive Doppler filtering algorithm is severely compromised at clutter edges, due to incorrect estimation of the clutter covariance matrix, and how in Space-Time Adaptive Processing a non-homogeneity detector can be used in the choice of the most appropriate STAP algorithm, forming the so-called Knowledge-Based STAP (KB-STAP) processor.

1. INTRODUCTION

The concept of adaptivity is central to the operation of modern radar signal and data processing. A single filtering, detection or tracking algorithm is not going to be optimum for all scenarios. Since Brennan and Reed's classic paper in 1973 [12], adaptive algorithms for detection, spatial filtering and Doppler filtering have been extensively studied and different algorithms have been devised to cope with different scenarios of targets, clutter and interference. At the same time, information theory tells us that prior knowledge can (and should) be used to reduce the uncertainty in processing decisions. In the radar context, such prior knowledge may take the form of information about the particular targets being sought, the inhomogeneity and topography of terrain, or meteorological conditions. Knowledge-based systems form part of the subject of artificial intelligence, in which a knowledge base is used to guide an inference engine to make its processing decisions. The concept, then, of knowledge-based signal processing is to make use of prior information in such a way as to choose the optimum processing method in each case.

Griffiths, H.D. (2006) Knowledge-Based Solutions as they Apply to the General Radar Problem. In *Knowledge-Based Radar Signal and Data Processing* (pp. 3-1 – 3-22). Educational Notes RTO-EN-SET-063 (2006), Paper 3. Neuilly-sur-Seine, France: RTO. Available from: http://www.rto.nato.int/abstracts.asp.

We interpret the 'general radar problem' as being the radar detection, classification and tracking of targets against a background of clutter and interference, with acceptable probabilities of detection and of false alarm. The radar may be terrestrial, maritime, airborne or space-based. We will assume in general that the radar will utilise a phased array antenna (linear or planar, or even conformal), allowing electronic control of the radiation pattern on receive and possibly on transmit as well, and we assume that there is explicit control of the radar waveform(s) which will be generated digitally and which may be varied on a pulse-to-pulse basis, and that these waveforms may be of substantial bandwidth, giving high range resolution. As well as the radar waveform, the dwell time and the pulse repetition frequency (PRF) may also be varied.

Thus this tutorial will provide an introduction, successively, to the application of knowledge-based techniques to filtering and detection (including space-time adaptive filtering), the nature of clutter, and tracking, aiming to show why knowledge-based signal processing may be advantageous, and to set the scene for the subsequent tutorials covering CFAR detection, space-time adaptive processing, tracking, and emerging technologies.

2. FILTERING AND DETECTION

2.1 The Matched Filter

We recall here the classical theory of the matched filter [32]. The matched filter maximizes the ratio of peak signal power to mean noise power. Let the transmitted waveform be $u(t)$. Its spectrum $F(\omega)$ is

$$F(\omega) = \int_{-\infty}^{\infty} u(t) \exp(-j\omega t)\, dt \tag{1}$$

If the receiver transfer function is $H(\omega)$ the output signal from the receiver prior to envelope detection is

$$g(t) = \int_{-\infty}^{\infty} F(\omega) G(\omega) \exp(j\omega t)\, df \tag{2}$$

Let $g(t_0)$ be the maximum value of $g(t)$. The power spectrum of the noise at the output of the matched filter is:

$$g(\omega) = \frac{N_0}{2} |H(\omega)|^2 \tag{3}$$

where $N_0/2$ is the noise spectral density at the input. The average noise power is then:

$$N = \frac{N_0}{2} \int_{-\infty}^{\infty} |H(\omega)|^2\, df \tag{4}$$

The energy of the input signal can be written:

$$E = \int_{-\infty}^{\infty} u^2(t)\, dt = \int_{-\infty}^{\infty} |F(\omega)|^2\, d\omega \tag{5}$$

An optimum radar detector must maximize the ratio of peak signal power to mean noise power at its output:

$$\frac{\left|g\left(t_0\right)\right|^2}{N} = \frac{\left|\int_{-\infty}^{\infty} F\left(\omega\right) H\left(\omega\right) \exp\left(j\omega t_0\right) df\right|^2}{\frac{N_0}{2}\int_{-\infty}^{\infty} \left|H\left(\omega\right)\right|^2 df} \tag{6}$$

So we seek the receiver transfer function $H(\omega)$ which maximizes this ratio. This can be found using Schwartz's inequality:

$$\frac{\left|g\left(t_0\right)\right|^2}{N} \leq \frac{2E}{N_0} \tag{7}$$

The maximum output signal-to-noise ratio occurs when the two sides are equal, which is true only if:

$$H\left(\omega\right) = K\ F^*\left(\omega\right) \exp\left(-j\omega t_0\right) \tag{8}$$

where K is a constant (gain) and t_0 is the time delay through the filter.

This says that the frequency response of the matched filter is equal (apart from K and t_0) to the complex conjugate of the signal spectrum $F(\omega)$.

The impulse response of the matched filter is:

$$h\left(t\right) = K_2 u^*\left(t_0 - t\right) \tag{9}$$

which is a time-delayed inverse of the input waveform, multiplied by a simple gain constant.

The time-domain output is the convolution of the input signal with the impulse response, which is:

$$g_0\left(t\right) = \frac{1}{T}\int_{-T/2}^{T/2} f\left(\tau\right) f\left(\tau + t_0 - t\right) d\tau \tag{10}$$

which is the autocorrelation function of the input signal (in the absence of noise).

In summary:

- the matched filter maximizes the ratio of peak signal power to mean noise power;
- its frequency response is the complex conjugate of the spectrum of the input signal;
- its impulse response is the time-inverse of the input waveform;
- the matched-filtered output waveform is the autocorrelation function of the input waveform.

2.2 Equivalence of Time/Frequency and Angular/Aperture Domains

The matched filter for a sampled sinusoid consists of summing the samples with unit amplitude weighting, and the resulting time-domain output is:

$$h(t) = \sum_{n=1}^{N} a_n \exp(-j2\pi n / N) \tag{11}$$

It is easy to see that this is exactly equivalent to the sampling by a linear antenna array of an incoming sinusoidal waveform (Figure 1). The resulting radiation pattern of the array steered to the direction of incidence θ_0 has the familiar form:

$$D(\theta) = \frac{\sin\left(\frac{\pi N d}{\lambda}(\sin\theta - \sin\theta_0)\right)}{N\sin\left(\frac{\pi d}{\lambda}(\sin\theta - \sin\theta_0)\right)} \tag{12}$$

where N is the number of elements, λ is the wavelength and d is the interelement spacing.

Thus the array forms a spatial matched filter, matched to the direction of incidence θ_0. This illustrates the equivalence between on one hand the Fourier transform relationship between the time domain and frequency, and on the other the Fourier transform relationship between the aperture domain and the angular ($\sin\theta$) domain. Thus all of the processing techniques developed for time domain / frequency domain can equally be applied in the aperture domain / angular domain. These include:

- matched filtering (as described above);
- the effects of the sampling theorem (aliasing); in the angular domain aliasing results in *grating lobes*;
- formation of a set of orthogonal filterbank responses by the Discrete Fourier Transform [10, 11]; in the angular domain the equivalent process is carried out by the Butler Matrix producing a set of orthogonal beams [14];
- weighting to reduce sidelobes (at the expense of loss and of broadening of response); the same weighting functions (Taylor, Chebyshev, …) are usable;
- synthesis of a desired radiation pattern (or spectrum) from a uniformly-spaced set of aperture (or time series) samples [49];
- superresolution techniques;
- adaptive filtering.

2.3 Superresolution Techniques

'Superresolution' is a term used to describe a set of processing techniques which attempt to resolve signals of closer angular separation than the classical Rayleigh λ/D limit (where λ is the signal wavelength and D the array length). An intuitive demonstration that this can be done is provided by considering the 'tree' structure of phase shifters and combiners shown in Figure 2, and known as the 'Davies Beamformer' [17].

In 1979, Schmidt presented one of the earliest, and certainly one of the best-known of the superresolution algorithms, which he named MUltiple SIgnal Classification, or MUSIC [36]. A similar formulation had been published earlier the same year by Bienvenu [7].

Consider an M-element array of arbitrary geometry, with n incident signals $F_1, F_2, \ldots, F_n$ ($n \leq M$). The element signals $X_1, X_2, \ldots, X_M$ can be written as

$$\begin{array}{ccccccccccc} X_1 & = & a_{11}F_1 & + & a_{21}F_2 & + & \ldots & + & a_{D1}F_n & + & W_1 \\ X_2 & = & a_{12}F_1 & + & a_{22}F_2 & + & \ldots & + & a_{D2}F_n & + & W_2 \\ \vdots & = & \vdots & + & \vdots & + & \ldots & + & \vdots & + & \vdots \\ X_M & = & a_{1M}F_1 & + & a_{2M}F_2 & + & \ldots & + & a_{DM}F_n & + & W_M \end{array}$$

or in matrix notation

$$\mathbf{X} = \mathbf{AF} + \mathbf{W} \tag{13}$$

Here the terms $W_1, W_2, \ldots W_M$ represent the noise at the array elements. This noise may be either internally or externally-generated.

The matrix **A** is known as the *array manifold*, and its coefficients depend on the element positions and directional responses. The j^{th} column of **A** is a mode vector **a**(θ) of responses of the array to the direction of arrival θ_j The mode vectors and **X** can each be visualized as vectors in M-dimensional space, and **X** is a linear combination of mode vectors, where the coefficients are the elements of **F**.

The covariance matrix **R** is formed by averaging a number of 'snapshots' of the element signals

$$\begin{aligned} \mathbf{R} &= \overline{\mathbf{X}\mathbf{X}^*} \\ &= \mathbf{A}\overline{\mathbf{F}\mathbf{F}^*}\mathbf{A}^* + \sigma^2\mathbf{I} \end{aligned} \tag{14}$$

under the assumption that the signals and noise are uncorrelated, and where the elements of the noise vector **W** are zero mean and of variance σ^2.

The covariance matrix can be broken down into its eigenvectors and eigenvalues

$$\mathbf{R} = \sum_{i=1}^{N} \lambda_i \mathbf{e}_i \mathbf{e}_i^* = \mathbf{ELE}^* \tag{15}$$

The eigenvalues λ_i of the covariance matrix will be

$$\lambda_i > \sigma^2 \text{ for } i = 1, \ldots, n, \text{ and } \lambda_i = \sigma^2 \text{ for } i = n+1, \ldots, M \tag{16}$$

The number of incident signals can therefore be determined by inspection of the relative magnitudes of the eigenvalues, or in some situations this information may be known *a priori*.

Consequently, the covariance matrix can be partitioned into an n-dimensional subspace spanned by the incident signal mode vectors and an M–n dimensional subspace spanned by the M–n noise eigenvectors

$$\mathbf{R} = \mathbf{E}_S\mathbf{L}_S\mathbf{E}_S^* + \mathbf{E}_N\mathbf{L}_N\mathbf{E}_N^* \tag{17}$$

where $\mathbf{E}_S$ is the M by n signal subspace and $\mathbf{E}_N$ is the M by M–n noise subspace.

The MUSIC algorithm then estimates the angular spectrum $P(\theta)$ of the incident signals according to

$$P(\theta) = \frac{1}{\mathbf{a}^*(\theta)\mathbf{E}_N\mathbf{E}_N^*\mathbf{a}(\theta)} \tag{18}$$

A large number of other superresolution algorithms have been formulated and evaluated, giving improved performance over the basic MUSIC algorithm. These include search-free methods such as ESPRIT (Estimation of Signal Parameters by Rotational Invariance Technique) and TAM, one-dimensional parameter search methods such as MUSIC and Capon's MVDR, and multidimensional search schemes such as IMP (Incremental MultiParameter), stochastic and deterministic max-likelihood, and WSF. Algorithms of this kind are described in detail in reference [25].

Figure 3 shows an attempt to classify these algorithms, into those which work with arrays of arbitrary geometry and those which are formulated for uniformly-spaced linear arrays. The algorithms are also divided into those based on translational invariance, one-dimensional parameter searches, and multi-dimensional parameter searches.

A particular problem occurs when the incident signals are correlated - such as would be the case with multipath, for example. In this case the MUSIC algorithm does not perform well, and a 'pre-whitening' process is necessary to decorrelate the input signals applied to the algorithm. This may be done by taking successive subaperture samples of the complete array, and using these as the inputs to the algorithm [38].

The description of superresolution presented here has been in terms of the aperture / angular domains, but clearly in view of the discussion of Section 2.2 the process can be applied equally in the time / frequency domains. It is interesting to note that the original description of the MUSIC algorithm includes the polarization domain as well [36].

2.4 Adaptive Filtering

The derivation of the matched filter in section 2.1 assumed a uniform noise distribution. We consider now the situation when the noise is inhomogeneous. Suppose we have an N-element array, of $\lambda/2$ spacing, in an environment of noise (interference and/or jamming) of which the angular distribution, in intensity, is fixed by a function $T(\tau)$ (where τ = sin θ). There is a wanted signal in the direction τ_0. The optimization criterion chosen here is to maximize the ratio between the array gain in this direction, $G(\tau_0)$, and the total noise power T_A received by the antenna. This ratio is sometimes called the 'factor of merit'

$$M = \frac{G(\tau_0)}{T_A} \tag{19}$$

The gain $G(\tau_0)$ is proportional to the square modulus of the characteristic function, which in turn is the Fourier Transform of the set of weight coefficients. We can therefore write:

$$G(\tau_0) = \left| \sum_1^N W_n \exp(j2\pi n\tau_0) \right|^2 \tag{20}$$

We define the 'weight matrix' or 'weight vector' by the column matrix

$$\mathbf{W} = \begin{bmatrix} W_1 \\ : \\ W_N \end{bmatrix} \tag{21}$$

The steering vector defining the pointing direction is written in the same way

$$\mathbf{D}_0 = \begin{bmatrix} 1 \\ \exp\left(j\pi\tau_0\right) \\ : \\ \exp\left(j\pi N\tau_0\right) \end{bmatrix} \tag{22}$$

The gain $G(\tau_0)$ is therefore written

$$G\left(\tau_0\right) = \left|\mathbf{W}^{\mathrm{t}}\mathbf{D}_0\right|^2 \tag{23}$$

(The symbol $\mathbf{W}^{\mathrm{t}}$ denotes the transpose of $\mathbf{W}$).

In the same way as the gain, the noise power received can be expressed in terms of the weight vector $\mathbf{W}$

$$\mathbf{S} = \sum_1^N s_n W_n \tag{24}$$

The set of element signals is

$$\boldsymbol{\sigma} = \begin{bmatrix} s_1 \\ : \\ s_N \end{bmatrix} \tag{25}$$

so we can write

$$\mathbf{S} = \boldsymbol{\sigma}^{\mathrm{t}}\mathbf{W} = \mathbf{W}^{\mathrm{t}}\boldsymbol{\sigma} \tag{26}$$

The noise power is therefore

$$T_A = \overline{\left|\mathbf{S}\right|^2} = \overline{\mathbf{S}^*\mathbf{S}} = \overline{\left(\mathbf{W}^{\mathrm{t}}\boldsymbol{\sigma}\right)\boldsymbol{\sigma}^{\mathrm{t}}\mathbf{W}} = \mathbf{W}^{\dagger}\overline{\boldsymbol{\sigma}^*\boldsymbol{\sigma}^{\mathrm{t}}}\mathbf{W} \tag{27}$$

where $\mathbf{W}^{\dagger}$ is the adjoint matrix of $\mathbf{W}$.

The covariance matrix $\mathbf{R}$ can be recognized in the product $\overline{\boldsymbol{\sigma}^*\boldsymbol{\sigma}^{\mathrm{t}}}$, thus

$$\overline{\boldsymbol{\sigma}^{*}\boldsymbol{\sigma}^{t}} = \overline{\begin{bmatrix} s_1^{*} \\ s_2^{*} \\ \vdots \\ s_N^{*} \end{bmatrix} \begin{bmatrix} s_1 \ \ldots \ s_N \end{bmatrix}} = \begin{bmatrix} \overline{|s_1|^2} & \cdots & \overline{s_1^{*} s_N} \\ \vdots & & \vdots \\ \overline{s_N^{*} s_1} & \cdots & \overline{|s_N|^2} \end{bmatrix} = \mathbf{R} \tag{28}$$

The factor of merit is therefore written

$$M = \frac{G(\tau_0)}{T_A} = \frac{\left|\mathbf{W}^{t}\mathbf{D}_0\right|^2}{\mathbf{W}^{\dagger}\mathbf{R}\mathbf{W}} \tag{29}$$

The problem of the optimum array is now to find a weight vector $\mathbf{W}$ which maximizes the factor of merit M. This reduces to finding the vector $\hat{\mathbf{W}}$ such that the factor of merit is stationary with respect to a perturbation dW. The solution is:

$$\mathbf{R}\hat{\mathbf{W}} = k\mathbf{D}_0 \tag{30}$$

where k is an arbitrary scalar constant.

If the covariance matrix can be inverted, we obtain

$$\hat{\mathbf{W}} = k\mathbf{R}^{-1}\mathbf{D}_0 \tag{31}$$

This says that the optimum weight vector is obtained by forming an estimate of the covariance matrix, inverting it, and multiplying by a steering vector to define the required direction of maximum gain. The estimate of the covariance matrix is formed by averaging a number of 'snapshots' of the element signals, and Reed, Mallett and Brennan [35] showed that the number of samples K must be such that

$$K \geq (2N - 3) \tag{32}$$

This is sometimes known as 'Brennan's law'.

Although this discussion has been in terms of the radiation pattern of an adaptive antenna array, the discussion of section 2.2 shows that it is equally applicable to adaptive Doppler filtering. This formed the basis of Brennan and Reed's classic 1973 paper [12].

2.5 Space-Time Adaptive Processing

Space-Time Adaptive Filtering (STAP) is a two-dimensional combination of adaptive antenna array and adaptive Doppler filtering to suppress clutter and jamming [27]. Figure 4 shows a sideways-looking airborne radar, from which it can be seen that the Doppler shift associated with an echo from an angle θ from boresight is

$$f_D = \frac{2vf_0 \sin\theta}{c} \tag{33}$$

Figure 5 shows a two-dimensional plot of the clutter and jamming, as a function of angle (sin θ extending from −1 to +1) and of Doppler (extending from –PRF/2 to +PRF/2). There is a weak target at boresight, and it can be appreciated from the diagram that two-dimensional filtering is necessary to suppress the clutter and jamming to reveal the target.

The 'STAP data cube' (Figure 6) is thus used to estimate the covariance matrix. One important aspect of research into STAP techniques is to devise efficient ways of computing the inverse of the covariance matrix, since direct inversion is usually impractical. Reduced-dimension STAP (RD-STAP) is one such technique. Further such techniques will be described in the fifth lecture in this series.

3. CLUTTER AND DETECTION

3.1 Introduction

Radar clutter has been studied since the earliest days of radar. A proper knowledge of the statistics of radar clutter is essential in predicting radar detection performance, i.e. in ensuring correct setting of the detection threshold in CFAR (constant false alarm rate) processing, and in determining the clutter residue at the output of Doppler filter processors [8].

For radars of low or moderate resolution, Gaussian statistics have for many years given adequate results, both for land and sea clutter. However, for high resolution radars at low grazing angles, it has been found that clutter pdfs (probability density functions) deviate quite markedly from Gaussian, and consequently that the detection performance predicted by Gaussian clutter models does not agree well with practical experience. This is particularly true for the 'tails' of the distributions, which are exactly the parts which have the greatest effect on the false alarm rate. Furthermore, high spatial resolution radars may be able to exploit the spatial and temporal correlation properties of the clutter, so models which can take this into account can give superior performance. Various models have therefore been proposed and analyzed to give improved performance.

In addition, it is important to understand the effects of clutter inhomogeneities (edges) and discrete scatterers, and of range-ambiguous clutter [4]. The latter may be critical in evaluating the performance of naval radars operating in littoral environments. The fact that clutter can be so variable underlines the idea that knowledge-based techniques should be valuable in using prior information to bring the most appropriate detection algorithms to bear.

The next section provides a brief review of clutter models in current use.

2.2 Clutter Models

Rayleigh model: The simplest model for radar clutter assumes that the clutter echo is the sum of a large number of contributions of similar amplitude and random phase, in which case the Central Limit Theorem indicates that the in-phase (I) and quadrature (Q) components are independent and Gaussian-distributed, in which case the intensity follows a negative-exponential distribution:

$$f_E(x) = \frac{1}{\beta}\exp\left(-\frac{x}{\beta}\right) \tag{34}$$

and the corresponding pdf of the envelope-detected voltage z is Rayleigh:

$$f_R(z) = \frac{2z}{\beta}\exp\left(-\frac{z^2}{\beta}\right) \qquad z \geq 0 \tag{35}$$

Ricean model: If there is an additional non-random component in the clutter echo, the peak of the distribution is shifted so that the most probable value of the received power is not zero. The pdf of the detected envelope can be written as:

$$f(z) = \frac{z}{\psi_0} \exp\left(-\frac{z^2 + A^2}{2\psi_0}\right) I_0\left(\frac{zA}{\psi_0}\right) \tag{36}$$

where $I_0(.)$ is the modified Bessel function of order zero, ψ_0 is the variance of the noise, A is the amplitude of the coherent component, and the ratio of coherent to random scattering is proportional to A^2/ψ_0.

Lognormal model: The lognormal distribution is obtained from the normal distribution using the transformation $x = \ln(y)$. The pdf of the detected envelope is:

$$f(z) = \frac{2}{\sqrt{2\pi}\sigma z} \exp\left[-\frac{1}{2\sigma^2}\left(2\ln\frac{z}{z_m}\right)^2\right] \tag{37}$$

where z_m is the median value of z and σ^2 is the standard deviation of $\ln(z)$.

Weibull model: The Weibull pdf [37] is intermediate between the Rayleigh and lognormal distributions:

$$f_w(z) = \frac{\nu}{\beta}\left(\frac{x}{\beta}\right)^{\nu-1} \exp\left(-\left(\frac{x}{\beta}\right)^{\nu}\right) \tag{38}$$

where β is the scale parameter and ν is the shape parameter. For $\nu = 2$ the expression reduces to the Rayleigh case.

In the 1970s, much research was done on the non-Gaussian characteristics of high-resolution clutter. The lognormal distribution was found to give a better fit than the negative exponential distribution, but still fell short of describing adequately the single point statistics of coherent clutter.

Compound K distribution model: The K-distribution was originally devised in the context of optical scattering, and was subsequently applied in its compound from to radar sea clutter [40-46]. It consists of the product of a modulation component associated with the large scale structure (in the case of the sea surface this represents the long-wavelength swell waves) and Rayleigh-distributed speckle resulting from the coherent addition of contributions from the individual scatterers. More recently, the K-distribution has also been found to give an accurate representation of the statistics of texture in high-resolution SAR images of rural target scenes [34], and even of texture in high-resolution sonar images of the seabed [22].

The Rayleigh distributed speckle component is described by:

$$f(x|y) = \frac{\pi x}{2y^2} \exp\left(-\frac{\pi x^2}{4y^2}\right) \qquad \text{for } 0 < x < \infty \tag{39}$$

and the modulation component is described by the chi-distribution:

$$f(y) = \frac{2b}{\Gamma(\nu)}(b\nu)^{2\nu-1}\exp\left(-b^2y^2\right) \qquad \text{for } 0 < y < \infty \tag{40}$$

where b is a scale parameter and ν is a shape parameter.

Equations (39) and (40) are combined to yield the usual form of the compound K-distribution:

$$f(x) = \frac{4c}{\Gamma(\nu)}(cx)^{\nu} K_{\nu-1}(2cx) \tag{41}$$

where $c = b\sqrt{\frac{\pi}{4}}$ is a scale parameter, ν is the same shape parameter as the chi-distributed modulation, and $K_\nu(.)$ is the modified Bessel function of the third kind of order ν. The shape parameter ν expresses the 'spikiness' of the clutter. For $\nu = \infty$ the expression reduces to the Rayleigh distribution., Low values of shape parameter ν (<1) indicate spiky clutter.

3.3 Sea clutter

The properties of sea clutter will depend on a wide variety of parameters: : the radar parameters (frequency, polarization, resolution (in range and azimuth), incidence angle, …), and the surface parameters (wave height and wavelength, wind speed and direction, presence or absence of 'whitecaps', presence or absence of rainfall on the sea surface, …) and will depend on whether the sea surface is in the open ocean or in the littoral region. Figures 7 and 8 show photographs of the sea surface from Sennen Cove in Cornwall, UK, from which simultaneous radar data was gathered. In Figure 7, corresponding to a significant wave height of 4.3 m, the presence of whitecaps at once suggests that there are individual and discrete scattering events upon the relatively slow modulated surface. In heavier sea conditions (Figure 8), corresponding to a significant wave height of 6.1 m, the whitecaps dominate even more and considerable areas of the scene are shadowed.

The radar frequency was 9 GHz, and it operated in a staring mode, mounted on a clifftop with a grazing angle of 1.5˚. The range resolution is 6 m. Figure 9 shows 6 second blocks of data from this radar (at vertical polarization) as Weibull plots (logarithmic probability of occurrence versus amplitude), displaced for clarity. It is evident that neither the power nor the distribution is stable with time.

Observation of the Doppler spectrum suggests that the clutter returns consist of discrete scatterers with a characteristic lifetime. The upper plot of Figure 10 is a very high PRF Doppler trace over 60 seconds. A series of individual scatterers can be seen to be breaking away from the underlying modulated Doppler spectrum. The middle plot shows a distribution measure of the spikiness of the distribution using the normalised log estimate U. The lower plot shows the proportion of the tails of the Doppler spectrum above the noise level. In this case the underlying Doppler bin distribution is not spiky, rather it is non-stationary exponential.

As an example of the problems faced by a CFAR detector, Figure 11 shows the detection threshold set by Cell Averaging (CA), Cell Averaging Greater Of (CAGO) and Order Statistic (OS) processors operating on simulated K-distributed clutter with shape parameter ν = 0.5 (i.e fairly spiky). The number of reference cells is 32, and the threshold multiplier factor α is set to achieve $P_{fa} = 10^{-4}$. For the OS processor k is chosen as 20. A 15 dB clutter edge is located at range bin no. 240. A number of closely spaced targets of 16 dB signal-to-clutter ration are located between range bins 70 and 95, with isolated targets at range bins 150 and 230.

Several points can be noted. For the CA detector it is apparent that the closely spaced targets raise the detection threshold between range bins 60 and 110 so much that none of the targets are detected. The isolated target at range bin 150 is detected, but the presence of the clutter edge raises the threshold in the vicinity of range bin 240, thereby masking the target at range bin 230. Close examination of the figure also indicates that a false alarm will occur in range bin 246, due to the threshold being biased down by the low region of clutter power still within the CFAR window. It is evident that for the CAGO processor the closely spaced targets are even more comprehensively masked by each other. Again, the isolated target at range bin 150 is detected and the target at range bin 230 is masked by the clutter edge. The clutter spike at sample 246 does not, however, cause a false alarm in the CAGO processor. The OS processor can be seen to resolve the closely spaced targets and exhibits no discernable increase in the threshold in that region. The isolated target at range bin 150 is, of course, detected, and the target at range bin 230 is now detected and is not masked by the clutter edge. This is achieved at the expense of a false alarm at range bin 246 caused by the clutter edge, and almost another false alarm at sample 243. The choice of a higher value of k, around 27 or 28, would eliminate the false alarms at the clutter edge, but would extend the region of target masking caused by the clutter edge to the left, causing masking of the target at range bin 230. It is also apparent that in regions of homogeneous clutter the threshold is lowest for the CA processor and highest for the OS processor, reflecting the nominal loss for these respective processors.

3.4 Land clutter [9]

The properties of land clutter will depend on a wide variety of parameters: the radar parameters (frequency, polarization, resolution (in range and azimuth), incidence angle, …) as with sea clutter, and the surface properties (topography, dielectric properties, vegetation, moisture, wind speed and direction, time of day and season of year, …).

As an example, land clutter data from the BYSON radar has been analyzed [23]. The BYSON radar (now decommissioned) was located at the Malvern site (formerly RSRE, DERA; now QinetiQ), and provided a fully-instrumented flexible experimental facility. It used two modified Siemens Plessey AWS-5 naval radar transmitters, with digital waveform synthesis. The radar is depicted in Figure 12 and its parameters summarized in Figure 13.

Figure 14 shows an example of the result of fitting four of the clutter models described in section 3.2 to measured land clutter data. A number of techniques exist to fit models to measured data, and thereby to estimate the parameters of the model distributions. A standard approach is the maximum likelihood estimator, but no closed-form solution for the K-distribution has been found, so alternative techniques are required. In the work described here the downhill simplex method has been used [33], implemented in Mathematica. The goodness-of-fit in each case was evaluated by computing the mean square difference (MSD) between the model pdf and the measured data:

$$\mathrm{MSD} = \frac{1}{N}\sum_{i=1}^{N}\left(p\left(x_i\right) - f\left(x_i\right)\right)^2 \tag{42}$$

The target scene in this example corresponds to a region at a range of 71.6 km, including a television transmitter mast located at Litchfield. The model giving the best fit (lowest value of MSD) is highlighted. In all cases the K-distribution gives the best fit, and the K-distribution and Weibull models are noticeably superior to the other models. There is little difference between HH and VV polarizations.

Further analysis of the same data (Figure 15) with reference to the corresponding terrain height information (Figure 16) has shown that the clutter statistics can be highly variable [16]. The two swaths shown in Figure 15 include a number of man-made structures such as a motorway (highway) with metal lampposts, power pylons, and glasshouses. A likelihood ratio test for individual range cells was used to classify the

data as exponential clutter (largely shadow), positive values (areas more likely to be an edge), and negative areas (more likely to be IID K), and the result is shown in Figure 17. Many of the 'spiky' areas are related to man-made structures.

The Doppler spectrum of land clutter will depend on the motion of wind-blown trees and other vegetation [9].

3.5 Application of Knowledge-based Processing

The conclusion to be drawn from the preceding discussion is that radar clutter will in general be non-Gaussian and non-stationary both in time and in space. When interference and jamming are present the environment will be even more non-uniform.

Adaptive Doppler filtering of nonhomogeneous clutter: A study of the application of adaptive Doppler filtering to nonhomogeneous clutter [4] considered three types of inhomogeneity:

(i) clutter in which the amplitude and spectral width in each range bin are randomly drawn from spatially invariant parent populations of specified characteristics. This could represent, for example, high-resolution sea clutter or land clutter due to wind-blown fields or trees;

(ii) clutter edges, in which the clutter amplitude and/or spectrum exhibit a step change at some point in the range profile of the clutter. This could typically represent transitions between land and sea clutter or shadowed and illuminated surface clutter;

(iii) clutter which is essentially homogeneous but in which a small number of range bins are corrupted by returns with significantly different amplitude and spectral characteristics, representing point-clutter sources or extraneous targets.

The performance is characterized in terms of the improvement factor (IF) defined as:

$$\mathrm{IF} = \frac{(S/C)_{out}}{(S/C)_{out}} = \frac{\mathbf{w}^H \mathbf{s}\mathbf{s}^T \mathbf{w}}{\mathbf{w}^H \mathbf{R}\mathbf{w}} \tag{43}$$

where **R** is the covariance matrix, as before, **w** is the desired filter weight vector and **s** is the vector of target returns. The IF was calculated for eight edge scenarios, tabulated in Figure 18, and for number of reference bins K = 10, 20 and $K \rightarrow \infty$. The clutter is assumed to have a Gaussian spectrum, with spectral width given by its standard deviation σ_0:

$$H(f) = \frac{1}{\sqrt{2\pi\sigma_0^2}} \exp\left(\frac{-(f - f_c)^2}{2\sigma_0^2}\right) \tag{44}$$

In homogeneous clutter, as $K \rightarrow \infty$ the estimated covariance matrix tends to the exact description of the clutter in the test cell. However, in nonhomogeneous clutter, as $K \rightarrow \infty$ the estimated covariance matrix in general will differ from that in the test cell.

Figure 19 shows the loss in IF around the clutter edge scenarios of Figure 18, and show that the losses can be substantial. The paper [4] goes on to show that prefiltering MTI can restore some of this loss.

Inhomogeneity detector in Space-Time Adaptive Processing: A second example of radar operation in nonhomogeneous clutter environments is in Space-Time Adaptive Processing. A number of different STAP algorithms have been developed [1, 2], and it is evident that no one algorithm is optimal in all scenarios. As the previous example has shown, the way in which the covariance matrix is estimated can have a great influence on the performance.

The concept of Knowledge-Based STAP was therefore developed, in which several different STAP algorithms are provided, with knowledge-based selection of algorithm parameters and selection of secondary data. The selection of the appropriate STAP algorithm for a given scenario is made on the basis of a non-homogeneity detector [1], and Figure 20 shows the basic scheme. The KB-STAP scheme has been extensively evaluated using data from the MCARM testbed.

4. TRACKING

The process of tracking consists of associating a set of detections to a particular target. The detections may be those from a single sensor, or in the general case they may be from a network of different sensors. The classical approach to monosensor tracking follows the stages of track initiation, plot-track correlation, track prediction, track filtering and track termination [19]. Classically the filtering process is provided by the α–β tracker, in which running averages of target position and velocity are maintained, updated at regular intervals. The values of α and β control the 'time constants' of the running averages, and represent a compromise on one hand between the ability to suppress noise, and on the other hand the ability to track target manoeuvres.

It can readily be appreciated that the tracking process offers great scope for adaptive processing and for the use of prior knowledge. The Kalman filter [13] is perhaps a first stage in this; here the filter time constants are varied adaptively according to the target's manoeuvres. There are further possibilities in adaptively varying the filter update interval, and in filters such as the Interactive Multiple Model (IMM), Joint Probabilistic Data Association (JPDA) and Multi-Hypothesis Tracking (MHT). These algorithms will be covered in the tutorial on application of knowledge-based techniques to the tracking function.

5. CONCLUSIONS

This tutorial has attempted to provide an introduction to the application of knowledge-based processing to the general radar problem. We have described the nature of the general radar problem and the basic processing techniques that are used. The fundamental concepts of matched filtering, superresolution and adaptive filtering have been described, emphasizing the equivalence of time/frequency and aperture/angular domains, and introducing the concept of Space-Time Adaptive Processing.

We have described some of the statistical clutter models in common use. It should be emphasized that these are just models, and as such represent an idealization of reality; nevertheless, clutter models can be very useful in predicting radar detection performance. Some practical examples of sea clutter and of land clutter have been presented, which demonstrate quite vividly that clutter is in general non-Gaussian and non-stationary, both in time and space. It is hoped this makes the case for the application of knowledge-based signal processing techniques to the general radar problem.

The two examples of filtering in nonhomogeneous clutter environments are intended to illustrate this further, showing that the performance of the adaptive Doppler filtering algorithm is severely compromised at clutter edges, due to incorrect estimation of the clutter covariance matrix, and how in Space-Time Adaptive Processing a non-homogeneity detector can be used in the choice of the most appropriate STAP algorithm, forming the so-called Knowledge-Based STAP (KB-STAP) processor.

6. ACKNOWLEDGEMENTS

I gratefully acknowledge invaluable discussions with many people from whom I have learned much about radar and signal processing over the years. I would particularly like to mention Chris Baker, DEN Davies, Alfonso Farina, Richard Klemm, Simon Watts, Richard White and Mike Wicks. I am also grateful to the students with whom I have worked on these subjects over the years, in particular Brian Armstrong, Glen Davidson, Jonathan Dunlop and Dominic Walker, and to the organisations, including the UK Ministry of Defence, the UK Engineering and Physical Sciences Research Council, QinetiQ and its predecessors, BAE SYSTEMS, Thales Sensors and AMS, who have supported the various projects.

7. REFERENCES

1. Adve, R., Antonik, P., Baldygo, W., Capraro, C., Capraro, G., Hale, T., Schneible, R. and Wicks, M., 'Knowledge-base application to ground moving target detection', AFRL-SN-RS-TR-2001-185, September 2001.
2. Antonik, P., Shuman, H., Li, P., Melvin, W. and Wicks, M.C., 'Knowledge-based space-time adaptive processing, Proc. *IEEE Radar Conference*, Syracuse NY, May 1997.
3. Armstrong, B.C. and Griffiths, H.D., 'CFAR detection of fluctuating targets in spatially correlated K-distributed clutter'; *IEE Proc*., Vol.138, Pt.F, No.2, pp139–152, April 1991.
4. Armstrong, B.C., Griffiths, H.D., Baker, C.J. and White, R.G., 'Performance evaluation of adaptive optimal Doppler processors in heterogeneous clutter'; *IEE Proc. Radar, Sonar and Navigation*, Vol.142, No.4, pp179–190, August 1995.
5. Benjamin, R., *Modulation, Resolution and Signal Processing in Radar, Sonar and Related Systems*, Pergamon Press, 1966.
6. Benjamin, R. and Griffiths, H.D., 'Aperture-domain signal processing'; *Electronics and Communication Engineering Journal*, Vol.1, No.2, pp71–80, March/April 1989.
7. Bienvenu, G., 'Influence of the spatial coherence of the background noise on high resolution passive methods', *Proc. IEEE International Conference on Acoustics, Speech and Signal Processing*, Washington DC, IEEE Publication No. 79CH1379-7 ASSP, 2-4 April 1979, pp306-309.
8. Billingsley, J.B., Farina, A., Gini, F., Greco, M.V. and Verrazzani, L., 'Statistical analyses of measured radar ground clutter data', *IEEE Trans. Aerospace and Electronic Systems*, Vol.AES-35, No.2, pp579-593, 1999.
9. Billingsley, J.B., *Low Angle Radar Land Clutter: Measurements and Empirical Models*, SciTech / Peter Peregrinus, 2002.
10. Bracewell, R.N., *The Fourier Transform and its Applications*, second edition, McGraw-Hill, 1978.
11. Brandwood, D.H., *Fourier Transforms in Radar and Signal Processing*, Artech House, 2003.
12. Brennan, L.E. and Reed, I.S., 'Theory of adaptive radar', *IEEE Trans. Aerospace & Electronic Systems*, Vol.AES-9, No.2, pp237-252, March 1973.
13. Brookner, E., *Tracking and Kalman Filtering Made Easy*, Wiley-Interscience, 1998.
14. Butler, J.L., 'Digital matrix and intermediate frequency scanning', Chapter 3 in *Microwave Scanning Antennas*, Volume III, (R.C. Hansen ed.), Peninsula Publishing, 1985.
15. Davidson, G. and Griffiths, H.D., 'Wavelet detection of low observable targets within sea clutter', Proc. *RADAR 2002* Conference, Edinburgh; IEE Conf. Publ. No.490, pp238–242, 15–17 October 2002.
16. Davidson, G., Griffiths, H.D. and Ablett, S., 'Statistical analysis of high resolution land clutter', Proc. *RADAR 2002* Conference, Edinburgh; IEE Conf. Publ. No.490, pp434–438, 15–17 October 2002.
17. Davies, D.E.N., 'Independent angular steering of each zero of the directional pattern of a linear array', *IEEE Trans. Antennas & Propagation*, Vol. AP-15, March 1967, pp296-298.
18. Drabowitch, S., Papiernik, A., Griffiths, H.D., Encinas, J. and Smith, B.L., *Modern Antennas*, Chapman & Hall / IEEE MTT, ISBN 0 412 57910 3, 1997.
19. Farina, A. and Studer, F.A., *Radar Data Procesing: Introduction and Tracking* (vol.1), Research Studies Press, May 1985.
20. Farina, A., *Antenna-based Signal Processing Techniques for Radar Systems*, Artech House, 1991.
21. Goldstein, J.S., Guerci, J.R. and Reed, I.S., 'Advanced concepts in STAP', Proc. *IEEE International Radar Conference*, Washington DC, pp699-704, May 2000.
22. Griffiths, H.D., Dunlop, J. and Voles, R., 'Texture analysis of sidescan sonar imagery using statistical scattering models', *Proc. NATO Conference on High Frequency Acoustics in Shallow Water*, Lerici, Italy; SACLANTCEN Conference Proceedings CP-45 (N.G. Pace, E. Poulinquen, O. Bergem and A.P. Lyons eds), pp187–194, 30 June – 4 July 1997.
23. Griffiths, H.D., Fassi, C., Dunsmore, M., Ablett, S. and Walbridge, M., 'Statistical analysis of high resolution land clutter', Proc. *NATO Symposium on Low Grazing Angle Clutter: its Characterisation,*

Measurement and Application, Columbia, MD, USA, 25–27 April 2000; RTO-MP-60, AC/323(SET)TP/12, pp25.1 – 25.10, October 2000.
24. Guerci, J.R., Goldstein, J.S., Zulch, P.A. and Reed, I.S., 'Optimal reduced-rank 3D STAP for joint hot and cold clutter mitigation', Proc. *IEEE Radar Conference*, Boston, pp119-124, April 1999.
25. Haykin, S. (ed.), *Advances in Spectrum Analysis and Array Processing* (vols I and II), Prentice-Hall, 1991.
26. Jakeman, E. and Pusey, P.N., 'Statistics of non-Rayleigh microwave sea echo', Proc. *RADAR'77* Conference, IEE Conference Publication No.155, pp105-109, 1977.
27. Klemm, R., *Space-Time Adaptive Processing*, Peter Peregrinus, 1999.
28. Lee, P., Barter, J., Beach, K., Caponi, E., Hindman, C., Lake, B., Rungaldier, H. and Shelton, J., 'Power spectral lineshapes of microwave radiation backscattered from sea surfaces at small grazing angles', *IEE Proc. Radar, Sonar and Navigation*, Vol.142, No.5, pp252-258, 1995.
29. Lee, P., Barter, J., Caponi, E., Caponi, M., Hindman, C., Lake, B. and Rungaldier, H., 'Wind-speed dependence of small grazing-angle microwave backscatter from sea surfaces', *IEEE Trans. Antennas & Propagation*, Vol.44, No.3, pp333-340, 1996.
30. Lee, P., Barter, J., Lake, B. and Thompson, H., 'Lineshape analysis of breaking-wave Doppler spectra', *IEE Proc. Radar, Sonar and Navigation*, Vol.145, No.2, pp135-139, 1998.
31. Long, M.W., *Radar Reflectivity of Land and Sea*, second edition, Artech House, 1983.
32. Nathanson, F.E., *Radar Design Principles*, Second edition, p355 et seq., McGraw-Hill, 1990.
33. Nelder, , J.A. and Mead, R., 'A simplex method for function minimisation' *Computer Journal*, Vol.7, p308, 1965.
34. Oliver, C.J. and Quegan, S., *Understanding Synthetic Aperture Radar Images*, Artech House, 1998.
35. Reed, I.S., Mallett, J.D. and Brennan, L.E., 'Rapid convergence rate in adaptive arrays', *IEEE Trans. Aerospace & Electronic Systems*, Vol.AES-10, November 1974, pp853-863.
36. Schmidt, R.O., 'Multiple emitter location and signal parameter estimation', Proc. RADC Spectrum Estimation Workshop, RADC-TR-79-63, Rome Air Development Center, Rome, NY, USA, Oct 1979, pp243-258; reprinted in *IEEE Trans. Antennas & Propagation*, Vol. AP-34, March 1986, pp276-280.
37. Sekine, M. and Mao, Y., *Weibull Radar Clutter*, Peter Peregrinus, 1990.
38. Shan, T.J. and Kailath, T., 'Adaptive beamforming for coherent signals and interference', *IEEE Trans. Acoustics, Speech & Signal Processing*, Vol. ASSP-33, No. 3, pp527-536, June 1985.
39. Van Trees, H.L., *Detection, Estimation and Modulation Theory, Part I*, Wiley, New York, 1968.
40. Walker, D., 'Experimentally motivated model for the low grazing angle Doppler spectra of the sea surface', *IEE Proc. Radar, Sonar & Navigation*, Vol.147, No.3, pp114-120, 2000.
41. Ward, K.D., 'Compound representation of high resolution sea clutter', *Electronics Letters*, Vol.17, No.16, pp561-563, August 1981.
42. Ward, K.D., 'A radar sea clutter model and its application to performance assessment', *Proc. RADAR'82* Conference, IEE Conference Publication No.216, pp203-207, 1982.
43. Ward, K.D. and Watts, S., 'Radar sea clutter', *Microwave Journal*, June 1985, pp109-121.
44. Ward, K.D., Baker, C.J. and Watts, S., 'Maritime surveillance radar, Part 1: radar scattering from the ocean surface', *IEE Proc.*, Vol.137, Pt.F., No.2, pp51-62, April 1990.
45. Watts, S., 'Radar detection prediction in sea clutter using the compound K-distribution model', *IEE Proc.*, Vol.132, Pt.F., No.7, pp613-620, December 1985.
46. Watts, S., 'Radar detection prediction in K-distributed sea clutter and thermal noise', *IEEE Trans. Aerospace & Electronic Systems*, Vol.AES-23, No.1, pp40-45, January 1987.
47. Watts, S., Baker, C.J. and Ward, K.D., 'Maritime surveillance radar, Part 2: detection performance in sea clutter', *IEE Proc.*, Vol.137, Pt.F., No.2, pp63-72, April 1990.
48. Wirth, W-D., *Radar Techniques using Array Antennas*, Peter Peregrinus, 2001.
49. Woodward, P.M., 'A method for calculating the field over a plane aperture required to produce a given polar diagram', *J.IEE*, Vol. 93, Pt. IIIA, pp1554-1558, 1946.
50. Woodward, P.M., *Probability and Information Theory, with Applications to Radar*, Pergamon Press, 1953; reprinted by Artech House, 1980.

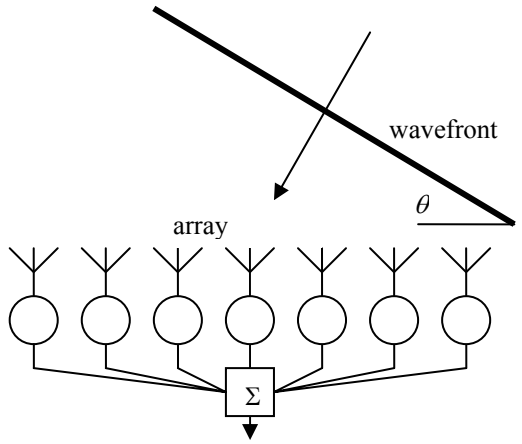

Figure 1. Linear antenna array as a spatial matched filter.

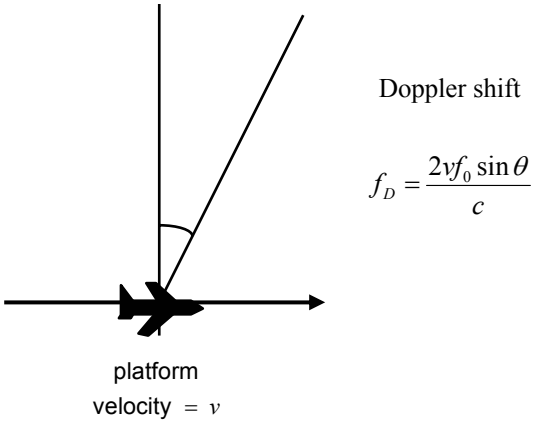

Figure 4. Doppler shift from a sideways-looking airborne radar.

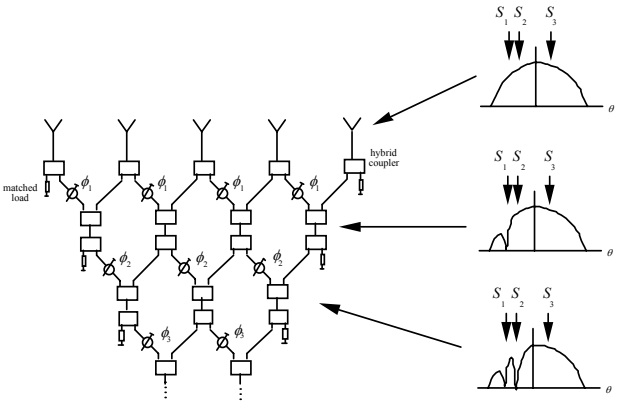

Figure 2. The Davies Beamformer.

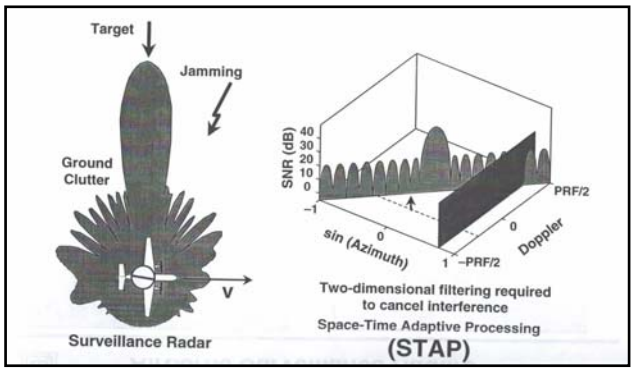

Figure 5. Space-Time Adaptive Processing (STAP): adaptive filtering in angle and in Doppler.

	Arrays of arbitrary geometry	Equi-spaced linear arrays
Translational invariance	ESPRIT [LS, TLS] †	TAM
One-dimensional parameter search	MVDR (Capon) MUSIC (Schmidt)	Maximum Entropy (Burg) minimum norm (KT)
Multi-dimensional parameter search	IMP (Clarke) WSF Stochastic max. likelihood Deterministic max. likelihood	† array must possess at least one translational invariance

Figure 3. Classification of superresolution algorithms.

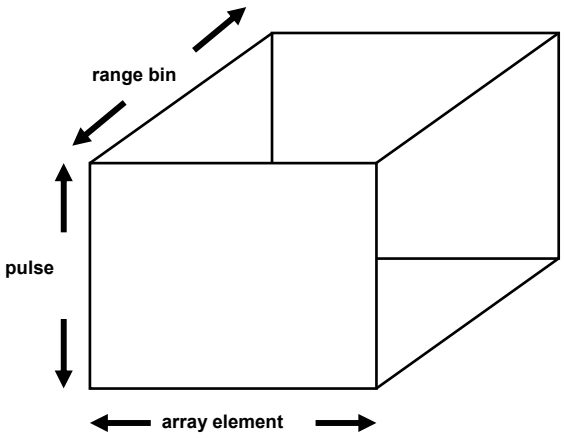

Figure 6. The STAP data cube.

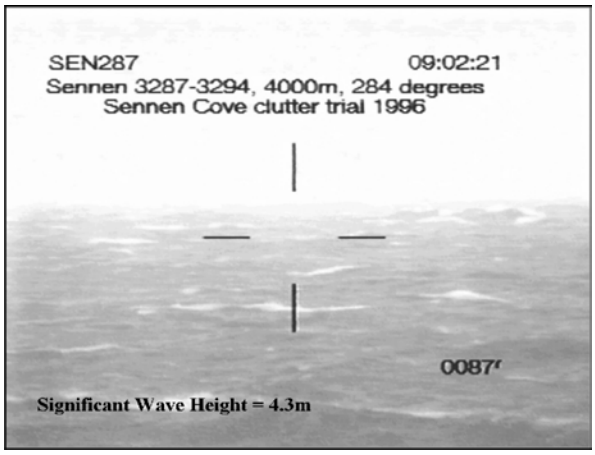

Figure 7. Photograph of sea surface from Sennen Cove, Cornwall, UK; significant wave height = 4.3 m.

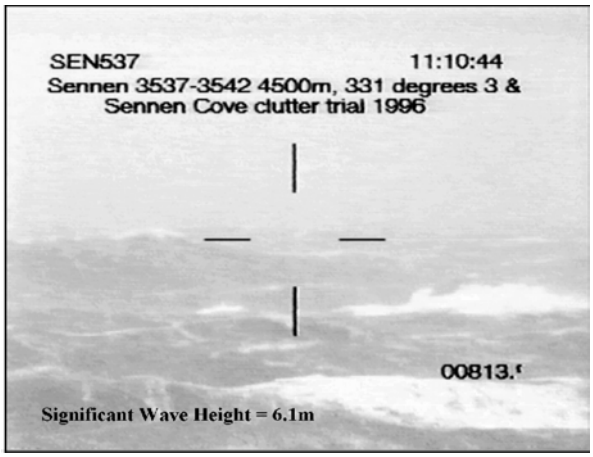

Figure 8. Photograph of sea surface from Sennen Cove, Cornwall, UK; significant wave height = 6.1 m.

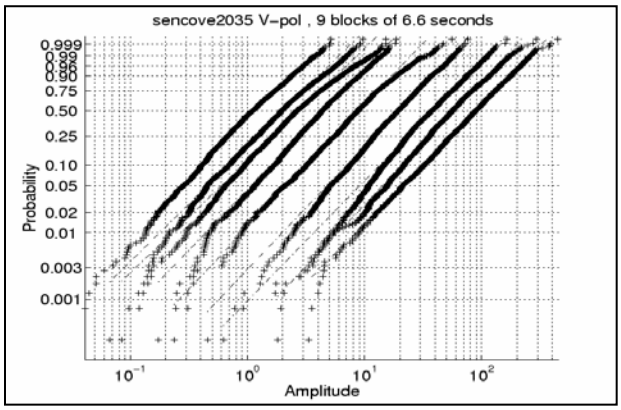

Figure 9. Consecutive Weibull plots of 6 second blocks of V-pol data, displaced for clarity. Neither power nor distribution is stable with time showing 2nd order statistics are necessary.

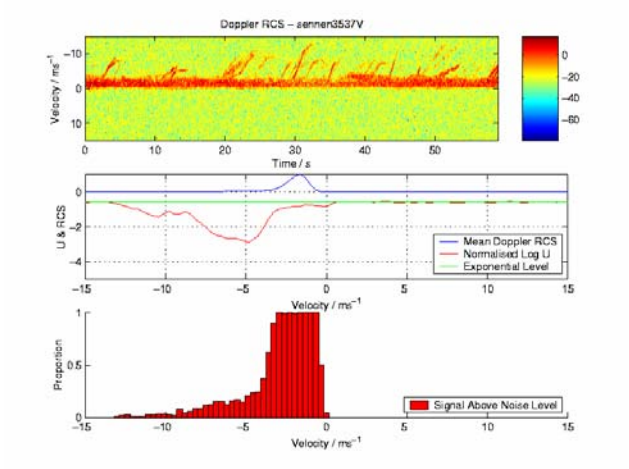

Figure 10. (a) High PRF Doppler trace over 60 second period; (b) distribution measure of spikiness; (c) proportion of tails of the Doppler spectrum above noise level [15].

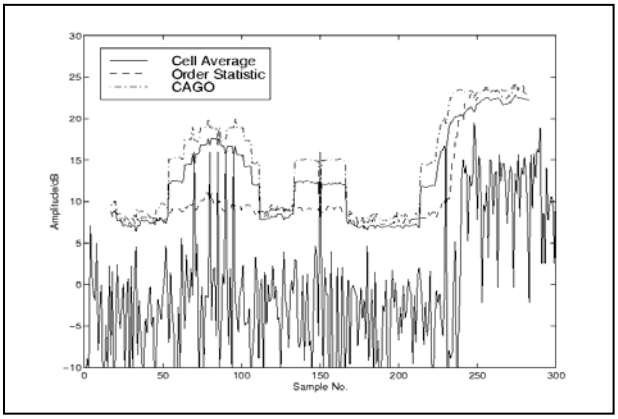

Figure 11. K-distributed noise (ν = 0.5), 32 cell CFAR, 16dB targets multiple @ 70-90, isolated target @ 150, potentially masked @ 230 by 14dB edge at 240 onwards.

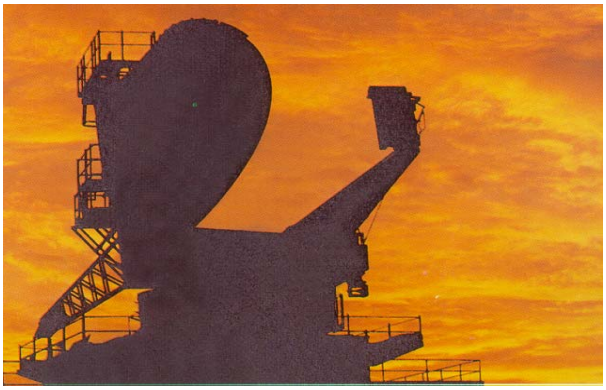

Figure 12. The BYSON radar.

frequency	2.7 – 3.1 GHz, frequency agile
PRF	100 Hz – 10 kHz
antenna gain	46 dBi
horizontal beamwidth	0.5°
vertical beamwidth	1.0°
polarisation	Vertical, horizontal or circular

Figure 13. BYSON radar parameters [23].

pol	dist	MSD	parameter values	
HH	Weibull	0.4487	β=7.03E-3	ν=1.5101
	lognormal	8.0164	σ^2=22.796	z_m=2.87E-6
	Ricean	1.6403	ψ_0=2.45E-2	A=3.017E-4
	K-dist	0.3254	ν=1.388	b=53.33
VV	Weibull	0.3969	β=0.0129	ν=1.429
	lognormal	6.0643	σ^2=20.33	z_m=5.18E-6
	Ricean	1.7269	ψ_0=0.031	A=3.05E-4
	K-dist	0.2729	ν=1.164	b=37.85

Figure 14. Fit of Weibull, lognormal, Ricean and K-distribution models to high-resolution land clutter data acquired using BYSON radar [23].

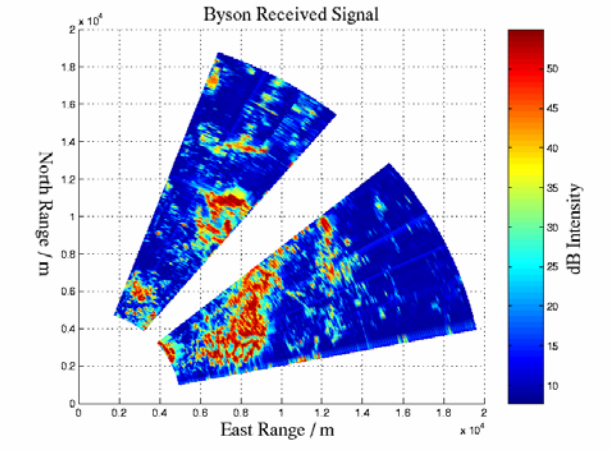

Figure 15. BYSON data (intensity in dB) [16].

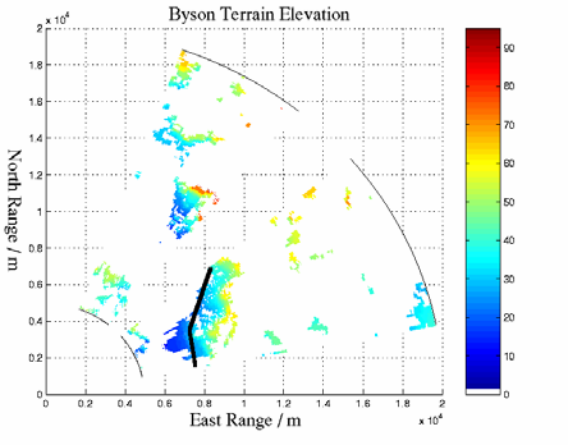

Figure 16. Digital elevation data corresponding to data of Figure 15 [16].

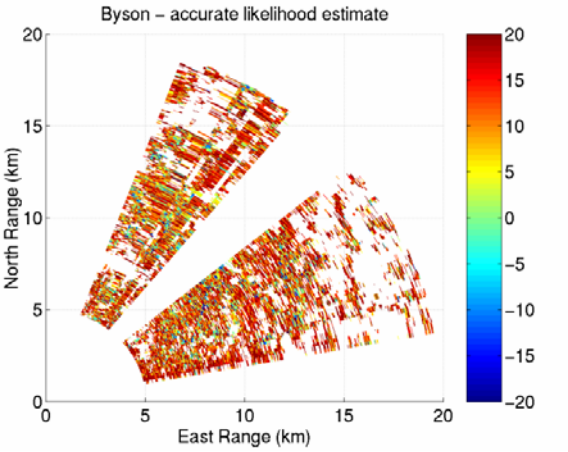

Figure 17. Likelihood ratio ($\log_{10}$) for individual range cells. White areas are classed as exponential clutter (largely shadow), positive values are more likely to be an edge, negative areas are more likely to be IID K. Note the motorway is visible as bright blue [16].

edge scenario	P_1	σ_1	f_{c1}	P_1	σ_1	f_{c1}
1	50	0.02	0	30	0.1	0.2
2	50	0.02	0	30	0.1	0.0
3	50	0.02	0	30	0.1	0.5
4	30	0.02	0	40	0.1	0.2
5	30	0.02	0	40	0.1	0.0
6	30	0.02	0	40	0.1	0.5
7	60	0.02	0	30	0.1	0.0
8	50	0.02	0	30	0.05	0.0

Figure 18. Clutter edge scenarios [4].

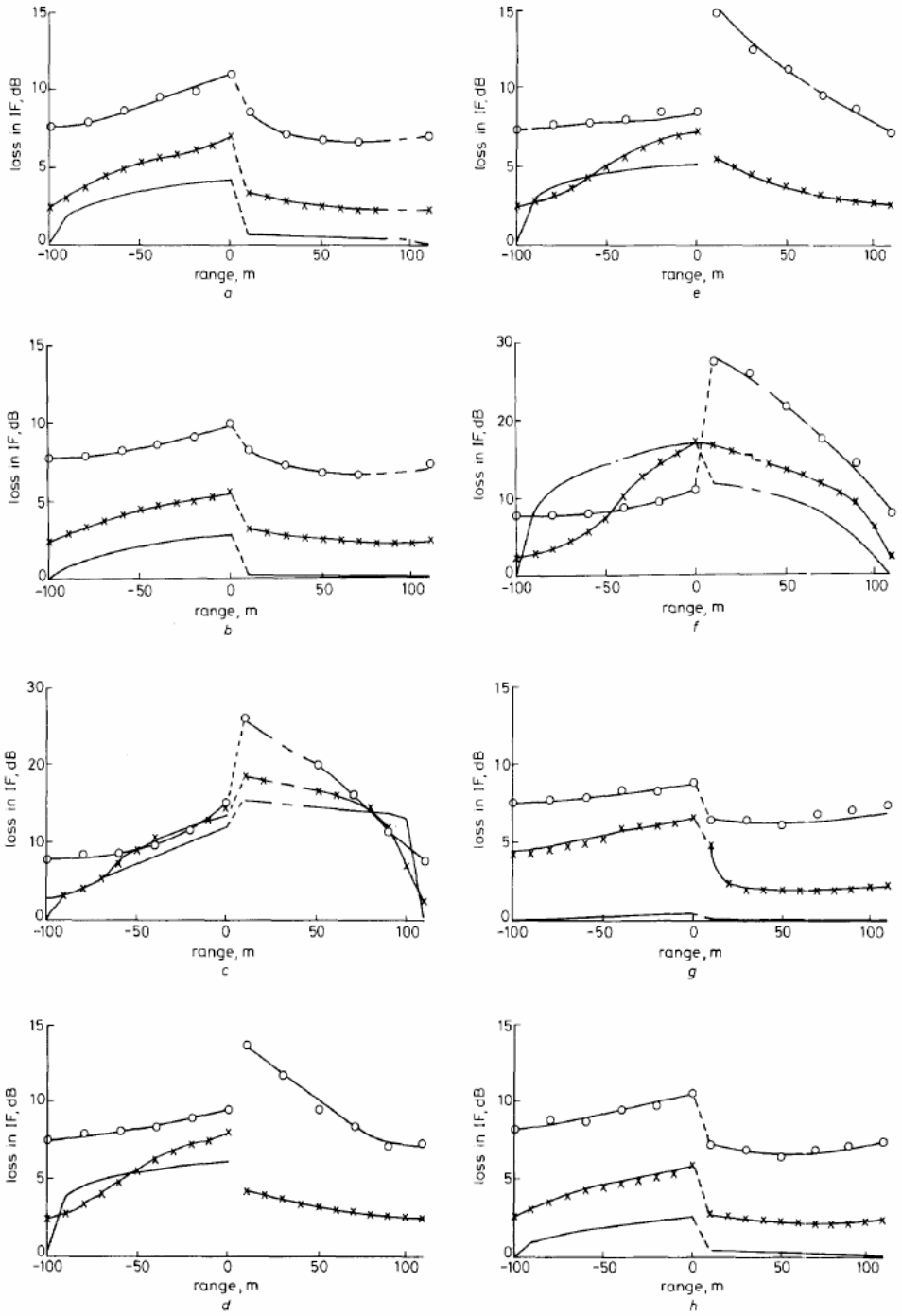

Figure 19. Improvement Factor (IF) loss around clutter edges ($N = 10$) (after [4]).

(a) edge scenario 1
(b) edge scenario 2
(c) edge scenario 3
(d) edge scenario 4
(e) edge scenario 5
(f) edge scenario 6
(g) edge scenario 7
(h) edge scenario 8

×-------× $K = 20$
o-------o $K = 10$
---------- $K \rightarrow \infty$

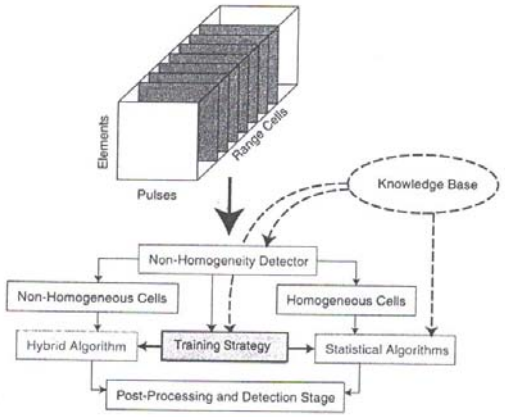

Figure 20. Knowledge-Based STAP (after [1]).